Improved Near-surface Wind Speed Characterization Using Damage Patterns

Daniel M. Rhee[1], Franklin T. Lombardo[1]
[1]University of Illinois at Urbana-Champaign, Urbana-Champaign, IL, USA

ABSTRACT: Tornadoes have caused significant damage and casualties in the past decades. These losses have spurred efforts toward tornado-based design, which require rigorous estimates of tornadic near-surface wind speeds. Due to difficulty of obtaining in-situ measurements and various issues regarding Enhance Fujita (EF) scale, a promising method of estimating near-surface wind speed based on damage inflicted is developed. The method utilizes fall directions of trees and other objects with distinct fall patterns to describe the characteristics of the tornado and other wind storms. The observed fall patterns are used to estimate Rankine vortex parameters and reproduce near-surface wind field. The wind field then can be compared to structural damage as an independent method. The near-surface wind speeds of different tornado cases were estimated using this method, one of which (Sidney, IL) exhibited 'crop-fall' patterns and yet another (Naplate, IL) had caused damage to trees and other infrastructures such as street signs. Based on the damage to structures and the estimated wind speeds from the tree-fall analysis, empirical fragility curves are also developed, which allows to interpret the vulnerability to tornadoes. The entire process of wind speed, wind load, structural resistance and ultimately how to mitigate damage then can be better understood.

KEYWORDS: Tornado, Wind speeds, Tree-fall, Crops, Fragility

1. INTRODUCTION

In the past two decades, annual average occurrence of over 1,200 tornadoes was reported in the United States (NOAA, 2018). These tornadoes have caused immense property damage and significant number of casualties. In recently years, the annual total loss due to these tornadoes has reached nearly $1 billion (Changnon, 2009). As a result, tornado-based design for all structures, including residential and commercial structures, is gaining traction in the engineering community in order to minimize structural damage (ASCE, 2016; Prevatt et al., 2012; van de Lindt et al., 2013). However, tornado-based design is particularly complicated because tornadoes induce more complex and extreme wind loading on buildings than straight-line winds (Amini and van de Lindt, 2013), and an inaccurate estimation wind speed can result a considerable error in wind-induced loading as the pressure is proportional to the wind speed squared. Thus, an accurate estimate of the near-surface wind field becomes an essential part of implementation of tornado-based design in codes and standards.

Despite the importance of accurate wind speed estimation, current methods of near-surface wind speed estimates have several difficulties and flaws. Although the recent development of portable radar measurements, such as DOW (Doppler On Wheels), has enabled full-scale tornado data collection (Refan et al., 2017), the radar measurements are limited in numbers and near-surface wind field is poorly understood due to noises and spurious data resulted from ground clutter and signal blockage near the surface (Oye et al., 1995). An alternate method of classifying tornado wind speed is through structural damage (e.g. F-scale, EF-scale), which is most commonly used in practice among engineers and meteorologists. However, there are lingering issues regarding inconsistency and subjectivity of wind speed estimation based on structural damage assessment. Doswell (1988) even states that “the F-scale is a damage scale, not an intensity (or windspeed) scale.” Although it is certain that structural damage and wind speed are correlated, the relationship between the two is much more complicated due to many factors, including the variability and subjective judgment in construction quality and type, different aerodynamic effects on shape of the structure, terrain effects, and etc. (Doswell, 2003; Edwards et al., 2013). As a result, a more rigorous method for estimating near-surface of tornadic wind speed independent of structural damage becomes necessary. Furthermore, the majority of the world’s tornadoes occur in open plains with low population density and therefore structure density is relatively low (Guyer and Moritz, 2003). This makes EF-scale estimation difficult and thus tornadoes are often underrated in rural areas due to the lack of number of structures (Edwards et al., 2013).

Due to frequent strikes of tornado and the lack of structures in crop fields, Fujita stresses the reliability and importance of crop damage pattern in his study of the Plainfield, IL tornado of 28 August 1990. Fujita (1993) exhibits several aerial photographs of various corn damage patterns: “comma-shaped”, “swirling”, “Eye-shaped” patterns, which can be used to illustrate the characteristics of tornadoes and downbursts. Different sizes and patterns of the corn damage provide information on size of the tornado core and formation of suction vortices. Some of these patterns can be produced numerically and used to describe the characteristics of tornadoes. A more detailed investigation of these patterns from Plainfield, IL will be discussed in a later section.

Fragility functions, which are probability functions of exceeding certain limit state at a given wind speed, can provide quantitative insight on how a structure fails under different conditions. These fragility functions have been commonly developed analytically in the past (Amini and van de Lindt, 2013; Ellingwood et al., 2004; Lee and Rosowsky, 2005; Rosowsky and Ellingwood, 2002). However, recent tornado-based design paradigms propose design based on limit states (Prevatt et al., 2012; van de Lindt et al., 2013), in which a performance-based design (PBD) approach becomes necessary. Recently, an empirical approach of building fragility functions was adopted, using numerically reproduced wind fields (Nishijima, 2012; Roueche et al., 2017), and the tree-fall analysis has been used as one of the tools to estimate the near-surface tornadic wind fields. Also, these empirically derived tornado fragility curves can be compared to straight-line wind fragility curves to visualize the difference in failure.

In this paper, a robust method of estimating near-surface tornadic wind speed using tree-fall and crop patterns is discussed. The method analyzes fall direction and swath of trees and crops that describe the characteristics of the tornado. The Rankine vortex (RV) parameters are estimated based on the fall patterns and the near-surface wind field is reproduced (i.e. tree-fall analysis). The authors seek to demonstrate the potential of tree-fall analysis and its future work for improvement through discussion of methodology and general framework. In application, the tree-fall analysis is first applied to different tornado cases and the numerical wind field of each tornado is generated using the vortex parameters that characterize the tornado. Then, comparison between wind speed estimate from the tree-fall analysis and estimate from structural damage and other wind indicators is examined. Lastly, empirical fragility curves are built using the wind speed estimated from the tree-fall analysis.

2. METHODOLOGY

2.1. Tree-fall Analysis Method

2.1.1. General History and Development

Johannes Letzmann, who was a pioneer of tornado research and influenced by Alfred Wegener, attempted to construct a composite wind field of a translating vortex using the idea of superposition of rotational and translational velocities. Consequently, Letzmann determined the near-surface tornadic wind field and created hand-drawn hypothetical forest damage patterns (Peterson, 1992), which became the foundation of tornado wind field modeling using tree-fall pattern and influenced many modern tornado researchers in reconstructing tornadic wind fields. For example, Holland et al. (2006) adopted Letzmann's model, combined with a tree resistance model to wind by Peltola et al. (1999), and generated analytical tree-fall patterns that could be used to assess storm characteristics. More recently, other researchers have compared the analytical patterns to actual observed patterns and estimated the near-surface wind speed of various tornadoes (Bech et al., 2009; Beck and Dotzek, 2010; Karstens et al., 2013; Lombardo et al., 2015). Other methods of estimating near-surface wind field using tree damage have also been developed. Independent of tornado vortex model, Godfrey and Peterson (2017) estimated the probability of trees blown down at different wind speed based on the wind resistance model by Peltola and Kellomäki (1993) and determined the EF-scale of forest damage.

2.1.2. Tree-damage Documentation (Tree-tagging)

Documentation of tree damage is an essential part of tree-fall analysis. Aerial photographs, which are often available, can display the tree damage pattern along the tornado track. With a Geographic Information System (GIS) software and high resolution aerial photographs, the geographic coordinates and fall direction of individual tree can be easily identified. Tree damage can be also documented in ground surveys. In general, the location and direction of trees in multiple transects are recorded using GPS unit cameras. Detailed ground survey is important because valuable tree information, unattainable from air, can be obtained from ground. Studies have shown that the tree-fall risk has a consistent relationship with tree size, species, and properties (Peterson, 2007), which are more easily identified on the ground. These values can provide better estimate on the critical wind speed of tree-fall, which is one of the important parameters used in the tree-fall analysis.

2.2. Tree-fall Analysis Inputs and Outputs

2.2.1. Rankine Vortex and Critical Wind Speed (Model Inputs)

Once the tree-fall patterns are documented, an idealized vortex model can be used to simulate the numerical tornado wind field and tree-fall patterns. A Rankine vortex (RV) model is a simple vortex model that is widely used to describe wind distribution of tornadoes and hurricanes

(Lewellen, 1993). The horizontal wind speed distribution of a stationary tornado has two regions: 1) a core region where the rotational wind velocity increases until the radius of maximum wind speed (RMW) and 2) an outer region with an exponential decay of velocity beyond RMW, as shown in Fig. 1. In equation, the rotational wind speed (V_{rot}) at different radius (r) is described as following:

$$V_{rot}(r) = V_{max}\left(\frac{r}{RMW}\right)^{\varphi} \quad \text{for } r \leq RMW$$

$$V_{rot}(r) = V_{max}\left(\frac{RMW}{r}\right)^{\varphi} \quad \text{for } r > RMW \qquad (1)$$

where φ is the decay exponent and V_{max} is the maximum speed at RMW. Typically, $\varphi = 1.0$ has been used in Letzmann's work and other studies (Beck and Dotzek, 2010). However, recent studies suggest that the decay exponent ranges between 0.5 and 0.8 based on Doppler radar data of tornadoes (Bluestein, 2007; Kosiba and Wurman, 2010, Wurman and Alexander, 2005). Example of normalized RV model with different exponents is shown in Fig. 1.

The rotational wind speed (V_{rot}) of tornado near surface can be decomposed to two components: the radial component (V_r) and tangential component (V_θ), as shown in Fig. 2. Although it is often assumed that the tornado flow field is dominated by the tangential component at higher elevation, there is a significant radial component due to a strong radial inflow near-surface (Gallus et al., 2004). The magnitudes of V_r and V_θ are determined by alpha (α), which is the angle between V_{rot} and V_r. The V_{rot} can be described purely radial and tangential at $\alpha = 0°$ and $\alpha = 90°$, respectively. Adding the translation speed of the tornado (V_T) to the V_{rot} yields the resultant wind speed (V) in the wind field at any radius. Fig. 2 illustrates the wind components and the resultant wind speed at a specific location. Typically, a constant translational speed is assumed in the analysis for simplicity and the storm motion from radar or ground observation is used as a proxy for tornado translation (Beck and Dotzek, 2010; Lombardo et al., 2015). However, if available, one may use a time varying translational speed. Karstens et al. (2013) estimated and used the translational speed of two tornadoes (Joplin, MO and Tuscaloosa-Birmingham, AL tornado) at different times based on the tornado vortex signature (TVS) positions.

Two additional parameters are used in the tree-fall analysis that determine the tree-fall pattern. The first parameter is G_{max}, which is the ratio between V_{max} and V_T. The equation for G_{max} is provided in Eq. (2).

$$G_{max} = \frac{V_{max}}{V_T} \tag{2}$$

The maximum resultant wind speed ($\hat{V}$) can be derived from G_{max} and V_T. For a point where $r = RMW$ and the V_T vector is aligned with the V_{max} (Fig. 2), the magnitude of two vectors can be summed to determine $\hat{V}$. The derivation of $\hat{V}$ is shown in Eq. (3).

$$\hat{V} = V_{max} + V_T = G_{max} \cdot V_T + V_T = V_T(G_{max} + 1) \tag{3}$$

The second parameter is the critical wind speed (V_c) at which a tree or crop will fall. It is assumed that the tree will fall in the direction of wind blowing at the instant when V exceeds V_c. In this study, an average value of V_c has been used. As mentioned in the earlier chapter, the critical wind speed of tree-fall information can be obtained in ground survey. Using the ground survey information, V_c can be determined with a mechanistic tree risk model by Peltola et al. (1993, 1999). There are also experimental means that can determine the V_c. Researchers in forestry have conducted winch tests, where trees are winched and the force required to overturn is measured by load cell, to determine tree resistance to overturning (Cucchi et al., 2004; Peterson and Claassen, 2012). Critical wind speed then can be estimated from the critical bending moment. Further, wind load on full-scale trees (i.e., real trees) at different wind speed was tested at Florida International University's Wall of Wind (WoW) (Aly et al., 2013). These experimental studies further extend investigation on the effects of soil type and soil-to-roots interaction. In addition to trees, the V_c of various crops has been modeled and tested in the agriculture field. The wind lodging of wheats in different conditions was examined using a portable wind tunnel (Berry et al., 2003; Sterling et al., 2003). Recently, a more generalized model of crop lodging that can be applied to wide range of crops has been developed (Baker et al., 2014), which can enable the application of tree-fall analysis in agricultural areas.

2.2.2. Tree-fall Patterns (Model Outputs)

Different combinations of the RV and V_c inputs produce different tree-fall patterns, which have several possible outputs. Examples of these outputs are damage width (*DW*), damage ratio (*DR*), and mean direction (*MD*). *DW* is the total width of the tree damage and *DR* is the ratio of *DW* on either side (i.e., south and north) of the convergence line in a given transect. Convergence line is defined as the estimated location where the tree-fall pattern converges to a line parallel to the tornado translating motion. However, tree-fall pattern may not always converge, resulting *DR* to be indeterminate, and thus *DR* may not be the most appropriate output to use. As *DR* may be undefined in some cases, an additional output, *MD*, is introduced. *MD* is the average tree-fall angle within certain spacing or bin and can be used for tree-fall patterns without a convergence line. Illustration of these outputs is shown in Fig. 3.

2.2.3. Output Comparisons

Once the outputs of the observed and simulated pattern are determined, the "best-matched" combination of parameters can be ascertained by comparing the outputs (*DW*, *DR*, and *MD*) of the two patterns. As opposed to scalar outputs (*DW* and *DR*), *MD* is a directional output and thus the cosine of the angle between the simulated and observed direction vector (i.e. unit vector) can be used for comparison. The cosine of the difference in angle is computed as shown in Eq. (4).

$$cos(\beta) = \frac{\overline{v_o} \cdot \overline{v_s}}{|\overline{v_o}| \cdot |\overline{v_s}|} = \overline{v_o} \cdot \overline{v_s} \quad (4)$$

Beta (β) denotes the angle between $\overline{v_o}$ and $\overline{v_s}$, which are the direction vector of observed and simulated, respectively. Since $\overline{v_o}$ and $\overline{v_s}$ are both unit vector, the denominator in the fraction is one and the final product of cos(β) becomes a simple dot product of two vectors.

In general, various different transects perpendicular to the tornado track are selected for comparison. The input parameters that define the tornado characteristics and the critical wind speed of tree-fall are used in a factorial design and the "best-matched" parameters are determined through multiple iteration process. In the initial process of parameter determination, an approximate range of the parameters is first estimated based on the overall tree-fall pattern and interaction plots (see Section 2.2.4). The initial range of estimated parameters are then prescribed into the vortex model that will generate different outputs. This process is iterated, comparing the outputs of the simulation and observation, until the parameter combination with minimum "error" in outputs is determined. Finally, the wind field that "best" represents the actual tornado wind field can be generated using the "best-matched" parameters. A schematic drawing of the tree-fall analysis process is shown in Fig. 4. Real-life applications of the tree-fall analysis are discussed in the later section.

There are other methods of comparing the observed and simulated pattern in other studies. Bech et al. (2009) and Beck and Dotzek (2010) compared the overall tree-fall pattern from the tornado to the simulated pattern. Although this method may be valid, one should take caution as different combination of parameters can produce similar pattern. In recent years, a more detailed comparison method was developed. Karstens et al. (2013) normalized the tree-fall directions by subtracting the estimated tornado translation direction, which were averaged in 100-m-wide bins. The mean cross section of the normalized direction plots for observed and simulated are then compared. More recently, Lombardo et al. (2015) used numerically defined outputs, such as the fall direction and the distance to the convergence line addition to the damage width (*DW*) and damage ratio (*DR*) of multiple cross section of Joplin, MO tornado for comparison.

2.2.4. General Tree-fall Pattern Examples

Examples of simulated tree-fall patterns and their outputs are discussed in this section. As an example, the tree-fall pattern changes significantly with two input parameters: G_{max} and alpha (α). In case of high G_{max} (generally 4.0-6.0), the rotational speed of the tornado is much greater than its translation speed and the trees are more likely to fall inward, towards the center of the vortex and the opposite direction of translation. On the other hand, a low G_{max} (generally 1.0-3.0) suggests a relatively higher translational speed and the trees are more likely to fall in the direction of translation for the same V_c. Examples of tree-fall patterns with two different G_{max} values are shown in Fig. 5a and 5b. As the G_{max} increases from 3.0 (Fig. 5a) to 4.5 (Fig. 5b) with a constant $\alpha = 0°$, an apparent change of tree-fall pattern and an increase in *DW* are noticed. If V_T is unchanged, Eq. 2 implies that an increase in G_{max} results an increase V_{max}, therefore causing more trees to fall. On the other hand, the damage ratio (*DR*) is unaffected by change in G_{max} (Fig. 5a-5b). With the convergence line located along the center of the tornado for both $G_{max} = 3.0$ and $G_{max} = 4.5$, the *DR* becomes 1.0 for both cases, as the damage width is the same on the south and the north side of the convergence line. The alpha (α) parameter also contributes significantly to the tree-fall pattern. As α increases from 0° to 90°, the simulated vortex flow changes from a pure radial flow to pure tangential flow. Unlike G_{max} parameter, α has a great effect on the *DR* due to the change in the vortex flow and little effect on the *DW*. It is evident that the *DR* increases significantly from 1.0 to 17.7 (Fig. 5b-5d) whereas the *DW* hardly changes. As α increases, the convergence line starts to shift north of the tornado center, causing *DR* to increase drastically. Eventually, the convergence line for $\alpha = 90°$ becomes undefined and the *DR* is no longer applicable (Fig. 5e). Note that *DR* is highly sensitive to grid spacing. Using a fine grid spacing is suggested as a more accurate *DR* will result though a prolonged computational time is expected. As smaller grid spacing is used, the *DR* should converge to a single value. A grid spacing of 0.05 miles was used for Fig 5.

Fig. 6 shows examples of tree-fall pattern generated at the beginning of the tornado simulation. These patterns resemble some of crop patterns that Fujita emphasizes in his study (Fujita, 1993). Represented by black arrow, the left figure of Fig. 6 resembles the "comma-shaped", and the right figure resembles the "swirling" pattern of crop damage in Fujita 1993. Alpha (α) = 45° and $\alpha = 90°$ were used for the "comma-shaped" pattern and the "swirling" pattern, respectively. These numerically simulated patterns show great potential in crop damage application.

More generally, different combinations of input parameters interact with each other differently and therefore produce different outputs. The relationships between different parameters and their interaction effects are shown in Fig. 7. The plots exhibit regression lines of percentage change of outputs (*DW* and *DR*) over the percentage change of different inputs. In Fig. 7 (left), it is evident that the *DW* increases as G_{max} and V_T increase, but decreases as φ and V_c increase. As a result, rapid increase in slope is noticed as G_{max} increases and V_c decreases. Intuitively, lower V_c would result an increase in *DW* since more trees would fall due to lower critical tree-fall wind speed. Fig. 1 illustrates a slower wind speed decay for lower φ, resulting a wider *DW*. Higher G_{max} and V_T contributes to higher maximum resultant wind speed ($\hat{V}$) (refer to Eq. (3)), thus increasing both G_{max} and V_T will increase the *DW* significantly. Although *DW* interaction is rather intuitive, the *DR* interaction is much more complicated and less intuitive because the convergence line (C.L) does not always exist. Furthermore, the position of the C.L is dependent on the tree-fall pattern and the size of *DW* on the north and south side (referred as DW_1 and DW_2 in Fig. 5), which are also dependent on the total *DW*. The interaction plots for *DR* with different G_{max}, α, and V_c are shown in Fig. 7 (right). One apparent notice is that *DR* increases significantly as α increases (as also shown in Fig. 5). For a low α (top row of Fig. 7), the slopes are rather flat, indicating that G_{max}, *RMW*, and V_c do not contribute significantly, but the interaction effects take place and the other parameters begins to contribute to the change in *DR* more as α increases. For high G_{max} and α and low V_c (blue line in bottom right figure of Fig. 7), the *DR* shows great sensitivity to the change in *RMW*, displaying almost a 120% increase (large negative slope). Note that these trends are valid only within the range of the parameter change and thus estimation outside of the parameter range should not be extrapolated. The trend and exact values are also subject to change for different reference parameters, but the general trend should be similar. These interaction plots can be useful for general interpretation of the RV and other parameters.

2.3. Model Supplements

Generally, a stationary vortex model is assumed to be symmetric in tornado wind field modeling. However, studies have shown that some tornadoes exhibit large asymmetry in wind field even with the translation speed subtracted, possibly due to additive effects of forward or rear flank down-draft (Doviak and Zrnić, 1993; Wurman and Gill, 2000). Thus, one way to compensate this is to divide the vortex model into quadrants with different parameters. Fig. 8 shows an example of RV model with different parameters in different quadrants. Varying parameters may allow to generate more realistic tree-fall pattern for some tornado cases.

Although the tree-fall analysis on different tornadoes in this study is based on the RV model, the RV model can be replaced with other tornado models, such as Burgers-Rott, Sullivan (Wood and Brown, 2011), and Houston-Powell model (Houston and Powell, 1994), to describe the wind profile. Furthermore, in-situ wind field measurements such as the radar velocity field, if available, can be incorporated into the tree-fall analysis. Refan et al. (2017) analyzed a series of radar data from multiple tornadoes using Ground-Based Velocity Track Display (GBVTD) analysis. The left figure of Fig. 9 is the azimuth wind field (at z = 43 m), including the tornado translation speed (24.5 mph), of the 2005 Stockton, KS tornado. The right figure of Fig. 9 shows fictitious tree-fall patterns that could have been produced by simulating this vortex. Refer to Refan et al. (2017) for detailed information about the radar measurements. Tree-fall analysis not only can be applied to tornadoes, but also to other wind storms with sufficient tree-fall data. By substituting the RV model with other wind field models, such as downburst model (Holmes and Oliver, 2000) and tropical cyclone model (Holland et al., 2010), the tree-fall pattern and near-surface wind field of other wind storms can be produced.

2.4. Other Techniques

In the past, tree identification and tagging (converting tree images to digital vectors) process has been carried out manually. However, for tornadoes with very large area of tree damage, tree identification becomes tedious and requires lots of manpower. With the recent development of advanced patterning recognition techniques, an automated tree identification process of detecting and tagging tree-falls in aerial photos can reduce the manual work significantly. Furthermore, using pre-simulated tree-fall patterns as a training set, machine learning technique can also extract "best-matched" parameters automatically without having to simulate tornado vortex and thus reduce the computational time. With these two techniques, from raw geo-located aerial photo to wind speed estimation, the whole process of estimating wind field can be entirely automated, creating a comprehensive "package", where meteorologists or engineers can use to estimate the near-surface tornadic wind speed.

3. APPLICATIONS

3.1. Application in Joplin, MO tornado

On the 22 May 2011, a devastating EF-5 rated tornado struck the city of Joplin, Missouri and caused 116 fatalities and nearly $2 billion total losses. The damage and location of nearly 1200 residential houses and the tree-fall direction and location of nearly 5000 trees were documented by ASCE and NIST respectively, as part of the post-storm inspection (Prevatt et al., 2013; Kuligowski et al., 2014). Several studies have analyzed the Joplin, MO tornado, using the tree-fall analysis, and simulated the near-surface wind field (Karstens et al., 2013, Lombardo et al. 2015). Lombardo et al. (2015) in particular makes a detailed spatial comparison between the EF scale rating from the damage survey and the estimated wind field. Furthermore, multiple empirical fragility curves (e.g. DODs, Roof failures) of Joplin, MO tornado were developed using the information obtained from ground survey and the wind speed estimated from tree-fall analysis (Roueche et al., 2017). These empirical fragility curves can be used to investigate the vulnerability for residential houses and different types of roof failure. Roueche et al. (2017) then compares the empirical fragility curves to the analytically derived fragilities using straightline winds (FEMA, 2012) and estimates the tornado load amplification factors (TLF).

3.2. Application in Naplate, IL tornado

On 28 February 2017, multiple tornadoes touched down in the state of Illinois and the eastern part of Missouri. The peak wind speed of the strongest tornado that struck Naplate, IL was estimated 155 mph by the National Weather Service (NWS) (NWS, 2017). A few days after the tornado, an exhaustive damage survey was conducted in the city of Naplate by the Wind Engineering Research Laboratory (WERL) at University of Illinois at Urbana-Champaign. Damage survey included documentation of the location and the Degrees of Damage (DOD) for FR12 (One- and Two-Family Residences); and the location (both standing and fallen) and fall direction of fallen trees. In addition, detailed dimensions and fall direction of other infrastructures, such as distribution poles and street signs, were measured. The post-damage map of data collected in survey is displayed on *ArcGIS* (Fig. 10). From the information from tree-fall and associate damage, the tornado center line (red line) and the approximate range of RV parameters (G_{max} and α) were then estimated. The tornado center line was first estimated based on the location where the residential house took the most damage and where the trees converged. In Fig. 10, the fallen trees near the tornado center point toward the direction of the tornado translation (red line), which roughly resembles the tree fall pattern in Fig. 5a. A low G_{max} (1.0-3.0) was estimated based on this observation. Further, more damage was inflicted on the south side than on the north side of the convergence line, which also allowed an initial estimate of α range. For the output comparison analysis, similar to the Joplin, MO tornado, the damage width (*DW*), damage ratio (*DR*), and Mean Direction (*MD*) were compared. The resulting "best-matched" parameters yielded hardly any difference in *DR* and *DW*, and an average 45.5° difference in *MD* where the average spacing was 100 m x 100 m bin. The storm motion of 23 m/s (51.4 mph), estimated by the Storm Prediction Center (SPC, 2017), was used for the translational speed in the analysis and the "best-matched" parameters (Table 1) were found based on the RV model. The wind field generated by the "best-matched" parameters is shown in contour in Fig. 10. It is evident that the wind speed was the highest, and thus caused the most damage, near the tornado center. The maximum wind speed estimated was 129 mph (EF-2) as opposed to 155 mph (EF-3) estimated by the NWS.

In the Tropical Cyclone Yasi report, failed and non-failed road signs ("windicators") are used to estimate the peak gust of the cyclone (Boughton et al., 2012). Some of the failed street signs that were inspected during the Naplate, IL damage survey and used to compare the estimated wind field. The failure wind speed of some of the street signs was calculated using the maximum bending moment of the posts. The detailed steps of analysis and equations can be found in the Yasi report (Boughton et al., 2012). An example of street sign failure is shown in Fig. 10. The maximum wind speed from the tree-fall analysis corresponding at the location of the failed street sign was 93 mph, and the failure wind speed of that street sign (with some uncertainty in the geometry) ranged between 82 and 100 mph. Another method to estimate wind speed using the ratio between standing trees and the fallen trees (Godfrey and Peterson, 2017) was applied to the Naplate, IL tornado and a maximum wind speed of 116 mph was estimated, resulting about 10% difference from the tree-fall analysis with RV model.

Empirical fragility curves were also developed using the maximum wind speed from the tree-fall analysis and the DODs of the residential houses collected from the survey. For each DOD, a binary damage state (0, 1) was assigned to each house with associated the maximum wind speed, and the lognormal best fit parameters were determined (Roueche et al., 2017). Then, the probabilities of structures meeting or exceeding a DOD at a given wind speed were determined as shown in Fig. 11. Due to insufficient data for the higher DODs, only DOD1 through DOD4 were constructed. The curves show an evident increase in mean failure wind speed with higher DODs. Comparing the fragility curves of Naplate tornado to those of Joplin tornado (Roueche et al., 2017), DOD1 and DOD2 display very similar curves, but the curves for DOD3 and DOD4 showed considerable difference (Fig. 11). The probability of meeting exceeding or exceeding DOD4 at wind speed of 150 mph is about 0.91 for the Joplin tornado, whereas the probability is about 0.68 for the Naplate tornado. Such difference may have occurred because much smaller sample size of DOD3 and DOD 4 in Naplate IL and lower maximum wind speeds from which the curves were conditioned. As stated previously, these fragility curves may be used to interpret the vulnerability of the residential houses to tornadoes.

3.3. Application in Tuscaloosa, AL

The wind distribution within a tornado is very complex due to its continuously varying structure (Grazulis, 2001). The tornado wind field varies spatially and temporally and thus tornado wind field models should be able to capture these variation in wind components (Banik et al., 2007). These changes in wind components often result change in tree-fall pattern along the track, which suggests spatially and temporally varying RV parameters in the tree-fall analysis. For example, the 27 April 2011, Tuscaloosa-Birmingham, AL tornado translated through the city of Tuscaloosa (approximately 7.5 miles) and caused severe structural and tree damage. A series of aerial photographs were acquired by the National Oceanic and Atmospheric Administration (NOAA) Remote Sensing Division, which are made available online by the Nation Geodetic Survey (NGS) (https://storms.ngs.noaa.gov/). The approximate ground sample distance (GSD) is 0.35 m per pixel. Approximately 6,000 fallen-trees in the city of Tuscaloosa were converted to digital vector on *ArcGIS*. Along the tornado track in the city, a significant change in tree-fall patterns was noticed, indicating spatially varying RV parameters as the tornado translates. A series of transects along the track displayed different tree-fall patterns and outputs were chosen and analyzed. Fig. 12 displays the digitally converted tree-fall direction and the tornado track with the analyzed transects. The tree-fall directions normalized by the direction of the tornado track were determined and color coded as denoted range in the legend. An apparent increase in the *DW* and change in tree-fall direction can be noticed along the tornado track. Early in the track, the trees appear to fall towards more perpendicular to the tornado track. Most of the normalized tree-fall direction within the range of 0°-45° and 315°-360° (red) and 135°-225° (blue), suggesting a strong radial flow. However, as the tornado translates along the track, a more rotational pattern starts to form as more trees start to fall within the range of 225°-3155° (black) near the center of the tornado track and 135°-225° (green) near the most south of the *DW*, indicating stronger tangential flow than earlier. Note that the normalized tree-fall direction is 0 due south respect to the direction of the tornado track, increasing counter-clockwise. The tornado track can be divided into multiple sections or transects and analyzed individually. This can provide detailed analysis of how the tornado characteristics and the wind field changed over time. The same tree-fall analysis method applied in the previous sections can be applied to determine them. In addition to the conventional RV model, azimuthally varying parameters in some sections can be utilized. In mountainous terrain, towards the end of the Fig. 12, tornadic damage patterns may have change because the topographic variation could influence the damage severity significantly (Cannon et al., 2016). On the top right corner of Fig. 12, the tornado exited the city and entered a region with significant terrain and topography. A number of trees that fell in the direction of the mountain ridges can be noticed. A special topographic effect should be considered when analyzing this region.

The Tuscaloosa-Birmingham, AL tornado had a damage path length of approximately 80.68 miles (NWS, 2011), damaging a large portion of heavily forested area. The aerial photos provided by the NGS have countless number of fallen trees. A detailed tree-fall analysis over a long span would be almost impossible with the traditional tree identification and tagging process. A case such as the Tuscaloosa-Birmingham, AL tornado would be an ideal case to utilize the patterning recognition and machine learning technique. With the help of supercomputing power, an automated tree-fall analysis can be done even for an astronomical volume of trees.

3.4. Application in Sidney, IL

Assessing tornadic damages and estimating near-surface wind speed in agricultural areas has been a challenge due to lack of structures. Fujita was a pioneer who conducted a detailed survey of wind storm damage (including a tornado) in crop fields. Fujita (1993) identified many unique crop-fall patterns (e.g. Fig. 5) that show great potential in near-surface wind speed estimation. However, there has not been any detailed studies looking at these crop-fall patterns since. On 9 September 2016 near Sidney, IL, an EF-2 rated tornado traversed over large field of mature soybeans and corns (NWS, 2016) and intriguing crop damage patterns that resembled tree-fall patterns were noticed, prompting WERL to conduct a ground survey and attempt to apply the tree-fall analysis in crop fields. Although the corns were harvested by the time of arrival, the location and direction of the soybean fall were recorded (red arrows in Fig. 12) and no structural damage was discovered in the vicinity. However, an interesting discovery in this particular damage survey was the formation of convergent and divergent patterns of soybeans. A convergent pattern (black arrows) was identified on the north side, and a divergent pattern (blue arrows) on the south side of the tornado center as shown in Fig. 12. An up-close photograph of the convergent pattern with diameter of approximately 2 m is shown on the top. It is speculated that these patterns illustrate possible indications of multiple vortices. Many studies have confirmed the existence of multiple vortices or small-scale vortices within a large vortex (Agee et al., 1975, 1977; Bluestein &

Pazmany, 2000; Fujita, 1970; Pauley and Snow, 1988). Wurman (2002) was able to obtain radar image of multi-vortices tornado using DOW and analyze them in more detail. Although the convergent and divergent patterns were found in field survey and inclusion of multiple vortices in the analysis could alter the result, they were not considered in this study. Low G_{max} (1.0-3.0) and α (0-20) were presumed initially as the larger scale soybean-fall pattern pointed toward the direction of the tornado translation and the damage on south and north side of convergence line was roughly the same. The SPC recorded a storm motion of 15.4 m/s (34.4 mph) (SPC, 2016), which was used in the simulated model and resulted the "best-matched" parameters (Table 1). The simulated crop-fall pattern (yellow arrow) and the resulting wind field (contour) are shown in Fig. 13. An EF-0 was rated in this particular location according to the NWS (NWS, 2016), whereas the maximum wind speed was estimated at 110 mph (EF-1) based on the crop-fall analysis. This supports the observation that EF-scale estimation is often underrated in agricultural areas and suggests that improvement of EF-scale or other means of wind speed estimation is essential. The patterns between the simulated and observed in Fig. 13 show good agreement though the outputs (DW and DR) produced up to 40% difference for some transects. Possible discrepancies could have been inherited from using a symmetric RV model and incorrect estimation of translation speed (V_T) and critical wind speed of soybean lodging (V_c). As stated in section 2.4, an asymmetric wind field could have exited in the tornado and may improve the result. Also, the translational speed used in the simulation was the averaged storm motion predicted by the NWS. However, it is possible that the instantaneous translational speed at the surveyed area was significantly different from the averaged storm motion. An accurate estimation of the critical lodging of crops is much more complex and requires numerous other parameters, such as soil strength, growth stage, rainfall, and etc. (Baker et al., 2014), which were not accounted in this analysis. Nonetheless, there some advantages in crop-fall analysis over tree-fall analysis. Some advantages of crop-fall analysis in agricultural area are: 1) the spacing between the crops are constant and 2) the crops have fairly uniform dimensions and properties compared to those of trees used in the tree-fall analysis. Despite the complexity, crop-fall analysis with further improvement demonstrates great potential in tornadic wind speed estimation in agricultural areas.

4. CONCLUSIONS

Wind speed estimation in tornadoes, due to their transience, intensity and complexity remains difficult. In many cases, tornadoes knock down a large volume of trees and provide valuable information on characteristics of the tornadoes. Tree-fall analysis utilizes the patterns of fallen trees during a tornado event and characterizes the patterns based on a translating Rankine vortex (RV) by comparing the outputs of the observed pattern to the simulated pattern. Using the estimated parameters, the near-surface wind field map of the tornado can be reconstructed and used as an independent method of wind speed estimation from structural damage. The estimated near-surface wind field then can be used to determine wind-induced tornado loading and other applications in tornado-based design. Empirical fragility curves can also be constructed based on the wind speed estimate and structural damage. The tree-fall analysis was applied to several different real-life tornadoes. The maximum wind speed estimation from tree-fall analysis on the Naplate, IL tornado yielded 129 mph (EF-2) as opposed to 155 mph (EF-3) by the NWS. The wind speed estimation was compared with other viable method, resulting maximum 12% difference in wind speed. Tree-fall analysis also has applications in risk and reliability studies. Empirical fragility curve uses the estimated near-surface wind field generated by tree-fall analysis and the damage assessment of nearby structures to predict the probability of failure. Comparison of the fragility curves between Naplate, IL and Joplin, MO tornado suggests that the residential houses experienced DOD1-2 performed roughly equally under tornado wind load although the DOD3-4 showed significant difference. For tornadoes that exhibit significant changes in tree-fall patterns along the track or within same transects, such as the Tuscaloosa-Birmingham, AL tornado, time varying or azimuthally varying parameters should be considered in the analysis.

Upon improvement, tree-fall analysis has vast potential and application. The RV model can be replaced with other severe wind storm models, such as downburst and tropical cyclone model, and the tree-fall analysis can be used to identify and estimate the wind field of other wind storm events. Tree-fall analysis demonstrates great potential in crop-damage as well. The 9 September, 2016 Sidney, IL tornado case was an unprecedented example of utilizing crop-damage to estimate near-surface tornado wind field in agricultural field. The crop-damage exhibited patterns similar to the tree-fall patterns, which led to attempt incorporation of tree-fall analysis in vegetation other than trees. The simulated soybean-fall pattern showed good agreement with the observed pattern. However, the model outputs had moderate differences. Other literature on crop research show highly complicated relationship between wind speed and crop-lodging. Further investigation on crops and improvement in the methodology is necessary to apply tree-fall analysis. Incorporating advanced pattern recognition and machine learning technique is another essential part of future tree-fall analysis. This can allow a rapid wind speed estimation of many different tornadoes, or different segments of a tornado, that can be widely adopted to the public or any other researchers.

Acknowledgments

The authors gratefully acknowledge the financial support of the VORTEX-SE program by NOAA (Award No: NA150AR4590228, NA16OAR4590219) to conduct multiple post-damage surveys and support the first author's doctorate program. Authors would also like to thank Maryam Refan for providing the GBVTD data and the members of Wind Engineering Research Laboratory (WERL) and other students at University of Illinois at Urbana-Champaign who assisted in the damage surveys.

REFERENCES

Agee, E., Church, C., Morris, C., Snow, J., 1975. Some synoptic aspects and dynamic features of vortices associated with the tornado outbreak of 3 April 1974. Mon. Weather Rev. 103 (4), 318-333.

Agee, E. M., Snow, J. T., Nickerson, F. S., Clare, P. R., Church, C. R., Schaal, L. A., 1977. An observational study of the West Lafayette, Indiana, tornado of 20 March 1976. Mon. Weather Rev. 105 (7), 893-907.

ASCE, 2016. Minimum design loads for buildings and other structures. Structural Engineering Institute. Reston, VA.

Aly, A. M., Fossati, F., Muggiasca, S., Argentini, T., Bitsuamlak, G., Franchi, A., Longarini, N., Crespi, P., Chowdhury, A. G., 2013. Wind loading on trees integrated with a building envelope. Wind Struct. 17 (1), 69-85.

Amini, M., van de Lindt, J., 2013. Quantitative insight into rational tornado design wind speeds for residential wood-frame structures using fragility approach. J. Struct. Eng. 140, 04014033.

Baker, C. J., Sterling, M., Berry, P., 2014. A generalised model of crop lodging. J. Theoret. Biol. 363, 1-12.

Banik, S. S., Hong, H. P., Kopp, G. A., 2007. Tornado hazard assessment for southern Ontario. Can. J. Civ. Eng. 34 (7), 830-842.

Bech, J., Gayà, M., Aran, M., Figuerola, F., Amaro, J., Arús, J., 2009. Tornado damage analysis of a forest area using site survey observations, radar data and a simple analytical vortex model. Atmos. Res. 93 (1), 118-130.

Beck, V., Dotzek, N., 2010. Reconstruction of near-surface tornado wind fields from forest damage. J. Appl. Meteorol. Climatol. 49 (7), 1517-1537.

Berry, P. M., Sterling, M., Baker, C. J., Spink, J., Sparkes, D. L., 2003. A calibrated model of wheat lodging compared with field measurements. Agricul. Forest Meteorol. 119 (3-4), 167-180.

Bluestein, H. B., 2007. Mobile Doppler radar observations of tornadoes. In: Preprints: Fourth European Conf. on Severe Storms, Trieste, Italy, ICTP/ARPA FVG, 2 pp., http://www.essl.org/ECSS/2007/abs/05-Radars/bluestein-1177432754.pdf.

Bluestein, H. B., Pazmany, A. L., 2000. Observations of tornadoes and other convective phenomena with a mobile, 3–mm wavelength, Doppler radar: The spring 1999 field experiment. Bull. Amer. Meteorol. Soc. 81 (12). 2939-2951.

Boughton, G. N., Henderston, D.J., Ginger, J.D., Homes, J.D., Walker, G.R., Leitch, C.J., Somerville, L.R., Frye, U., Jayasinghe, N.C., Kim, P.Y., 2012. Tropical cyclone Yasi: Structural damage to buildings. James Cook University.

Cannon, J. B., Hepinstall-Cymerman, J., Godfrey, C. M., Peterson, C. J., 2016. Landscape-scale characteristics of forest tornado damage in mountainous terrain. Landsc. Ecol. 31 (9), 2097-2114.

Changnon, S.A., 2009. Tornado losses in the United States. Natural Hazards Review. 10 (4), 145-150.

Cucchi, V., Meredieu, C., Stokes, A., Berthier, S., Bert, D., Najar, M., Denis, A., Lastennet, R., 2004. Root anchorage of inner and edge trees in stands of Maritime pine (Pinus pinaster Ait.) growing in different podzolic soil conditions. Trees, 18 (4), 460-466.

Doswell, C. A., 2003. A guide to F-scale damage assessment. NOAA Rep., 101 pp.

Doswell, C. A., Burgess, D. W., 1988. On some issues of United States tornado climatology. Mon. Weather. Rev. 116 (2), 495-501.

Doviak, R. J., D. S. Zrnić, 1993. Observation of winds, storms, and related phenomena, Doppler Radar and Weather Observations, 2nd ed., pp. 280–385, Dover, New York.

Edwards, R., LaDue, J.G., Ferree, J.T., Scharfenberg, K., Maier, C., Coulbourne, W.L., 2013. Tornado intensity estimation: past, present, and future. Bull. Am. Meteorol. Soc. 94 (5), 641-653.

Ellingwood, B. R., Rosowsky, D. V., Li, Y., Kim, J., 2004. Fragility assessment of light-frame wood construction subjected to wind and earthquake hazards. J. Struct. Eng. 130 (12), 1921-1930.

FEMA. 2012. Multi-hazard loss estimation methodology: Hurricane model technical manual. Hazus-MH 2.1–Technical manual. Dept. of Homeland Security. Washington, DC.

Fujita, T. T., 1970. The Lubbock tornadoes: A study of suction spots. Weatherwise. 23 (4), 161-173.

Fujita, T.T., 1993. Plainfield Tornado of August 28, 1990. The Tornado: Its Structure, Dynamics, Prediction, and Hazards. Geophys. Monogr. 79, Amer. Geophys. Union, Washington, DC, 1-17.

Gallus Jr., W.A., Sarkar, P.P., Haan Jr., F.L., Le, K., Kardell, R., Wurman, J., 2004. A translating tornado simulator for engineering tests: Comparison of radar, numerical model, and simulator winds. In: Preprints: 22nd Conf. Severe Local Storms, Hyannis, MA, American Meteorological Society.

Godfrey, C. M., Peterson, C. J., 2017. Estimating enhanced Fujita scale levels based on forest damage severity. Weather Forecasting, 32 (1), 243-252.

Grazulis, T. P., 2001. The tornado: Nature's ultimate windstorm. University of Oklahoma Press. Norman, OK.

Guyer, J.L., Moritz, M.L., 2003. On issues of tornado damage assessment and F-scale assignment in agricultural areas, In: Preprints: 83rd AMS Annual Meeting Symposium on F-scale and Severe-Weather Damage Assessment.

Holland, A.P., Riordan, A.J., Franklin, E.C., 2006. A simple model for simulating tornado damage in forests. J. Appl. Meteorol. Climatol. 45 (12), 1597-1611.

Holland, G. J., Belanger, J.I., Fritz, A., 2010. A revised model for radial profiles of hurricane winds. Mon. Weather Rev. 138 (12), 4393-4401.

Holmes, J. D., Oliver, S. E., 2000. An empirical model of a downburst. Eng. Struct. 22 (9), 1167-1172.

Houston, S. H., Powell, M. D., 1994. Observed and modeled wind and water-level response from Tropical Storm Marco (1990). Weather Forecasting. 9 (3), 427-439.

Karstens, C.D., Gallus, W.A., Lee, B.D., Finley, C.A., 2013. Analysis of tornado-induced tree fall using aerial photography from the Joplin, Missouri, and Tuscaloosa–Birmingham, Alabama, Tornadoes of 2011. J. Appl. Meteorol. Climatol. 52 (5), 1049-1068.

Kosiba, K., Wurman, J., 2010. The three-dimensional axisymmetric wind field structure of the Spencer, South Dakota, 1998 tornado. J. Atmos. Sci. 67 (9), 3074-3083.

Kuligowski, E.D., Lombardo, F.T., Phan, L.T., Levitan, M.L., Jorgensen, D.P., 2014. Technical investigation of the May 22, 2011, tornado in Joplin, Missouri. Natl. Inst. Stand. Technol. 428.

Lee, K. H., Rosowsky, D. V., 2005. Fragility assessment for roof sheathing failure in high wind regions. Eng. Struct. 27 (6), 857-868.

Lewellen, W. S., 1993. Tornado vortex theory. The tornado: Its structure, dynamics, prediction and hazards. Geophys. Monogr. 79, Amer. Geophys. Union, Washington, DC, 19-39.

Lombardo, F. T., Roueche, D. B., Prevatt, D. O., 2015. Comparison of two methods of near-surface wind speed estimation in the 22 May, 2011 Joplin, Missouri Tornado. J. Wind Eng. Ind. Aerodyn. 138, 87-97.

Nishijima, K., Maruyama, T., Graf, M., 2012. A preliminary impact assessment of typhoon wind risk of residential buildings in Japan under future climate change. Hydrol. Res. Lett. 6, 23-28.

NOAA, 2018. State of the Climate: Tornadoes for Annual 2017, <https://www.ncdc.noaa.gov/sotc/tornadoes/201713>, National Centers for Environmental Information.

NWS, 2011. Tuscaloosa-Birmingham Tornado - April 27, 2011, <https://www.weather.gov/bmx/event_04272011tuscbirm>, National Weather Service.

NWS, 2016. Summary of September 9th Tornadoes in East Central Illinois, <https://www.weather.gov/ilx/09sep2016-survey>, National Weather Service.

NWS, 2017. Severe Weather Event Review for Tuesday February 28, 2017, <http://www.spc.noaa.gov/exper/archive/event.php?date=20170228>, National Weather Service.

Oye, R., Mueller, C., Smith, S., 1995. Software for radar translation, visualization, editing, and interpolation. In Preprints, 27th Conf. on Radar Meteorology, Vail, CO, Am. Meteorol. Soc. 359-361.

Pauley, R. L., Snow, J. T., 1988. On the kinematics and dynamics of the 18 July 1986 Minneapolis tornado. Mon. Weather Rev. 116 (12), 2731-2736.

Peltola, H., & Kellomäki, S., 1993. A mechanistic model for calculating windthrow and stem breakage of Scots pines at stand age. Silva Fenn. 27 (2), 99-111.

Peltola, H., Kellomäki, S., Väisänen, H., Ikonen, V.-P., 1999. A mechanistic model for assessing the risk of wind and snow damage to single trees and stands of Scots pine, Norway spruce, and birch. Can. J. For. Res. 29 (6), 647-661.

Peterson, C. J., 2007. Consistent influence of tree diameter and species on damage in nine eastern North America tornado blowdowns. Forest Ecol. Manag. 250 (1-2), 96-108.

Peterson, C. J., Claassen, V., 2012. An evaluation of the stability of Quercus lobata and Populus fremontii on river levees assessed using static winching tests. Forestry. 86 (2), 201-209.

Peterson, R.E., 1992. Johannes Letzmann: a pioneer in the study of tornadoes. Weather Forecasting 7 (1), 166-184.

Prevatt, D.O., Coulbourne, W., Graettinger, A.J., Shiling, P., Gupta, R., Grau, D., 2013. Joplin, Missouri, Tornado of May 22, 2011: Structural Damage Survey and Case for Tornado-Resilient Building Codes. ASCE Publications.

Prevatt, D.O., van de Lindt, J.W., Back, E.W., Graettinger, A.J., Pei, S., Coulbourne, W., Gupta, R., James, D., Agdas, D., 2012. Making the case for improved structural design: tornado outbreaks of 2011. Leadersh. Manage. Eng. 12 (4), 254-270.

Refan, M., Hangan, H., Wurman, J., Kosiba, K., 2017. Doppler radar-derived wind field of five tornado events with application to engineering simulations. Eng. Struct. 148, 509-521.

Rosowsky, D. V., Ellingwood, B. R., 2002. Performance-based engineering of wood frame housing: Fragility analysis methodology. J. Struct. Eng. 128 (1), 32-38.

Roueche, D. B., Lombardo, F. T., and Prevatt, D. O., 2017. Empirical approach to evaluating the tornado fragility of residential structures. J. Struct. Eng. 143 (9). 04017123.

SPC, 2016. Tornado Watch 472, <http://www.spc.noaa.gov/products/watch/2016/ww0472.html >, Storm Prediction Center.

SPC, 2017. Severe Weather Event Review for Tuesday February 28, 2017, <http://www. spc.noaa.gov/exper/archive/event.php?date=20170228>, Storm Prediction Center.

Sterling, M., Baker, C. J., Berry, P. M., Wade, A., 2003. An experimental investigation of the lodging of wheat. Agricult. Forest Meteorol. 119 (3-4), 149-165.

van de Lindt, J.W., Pei, S., Dao, T., Graettinger, A., Prevatt, D.O., Gupta, R., Coulbourne, W., 2013. Dual-objective-based tornado design philosophy. J. Struct. Eng. 139 (2), 251-263.

Wood, V. T., Brown, R. A., 2011. Simulated tornadic vortex signatures of tornado-like vortices having one-and two-celled structures. J. Appl. Meteorol. Climatol. 50 (11), 2338-2342.

Wurman, J., 2002. The multiple-vortex structure of a tornado. Weather Forecasting. 17 (3), 473-505.

Wurman, J., Alexander, R.A., 2005. The 30 May 1998 Spencer, South Dakota, Storm. Part II: Comparison of observed damage and radar-derived winds in the tornadoes. Mon. Weather Rev. 133 (1), 97-119.

Wurman, J., Gill, S., 2000. Finescale radar observations of the Dimmitt, Texas (2 June 1995), tornado. Mon. Weather Rev. 128 (7), 2135-2164.

FIGURES

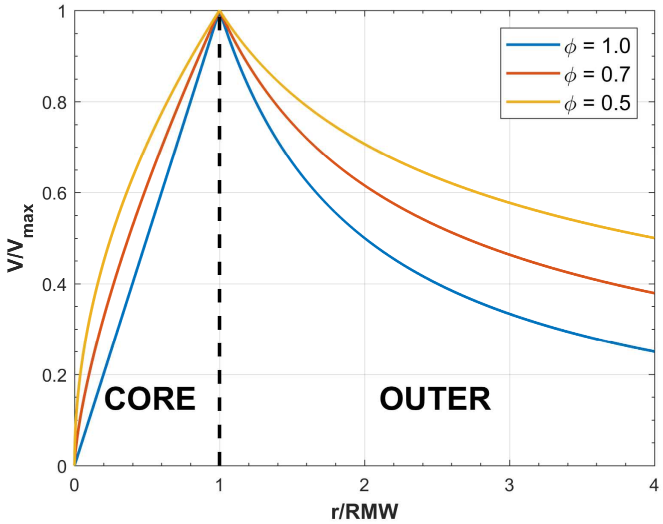

Figure 1. Normalized Rankine vortex (RV) model with different decay exponents. In the core region, the wind speed increases until (r/RMW = 1.0) and then decreases exponentially in the outer region.

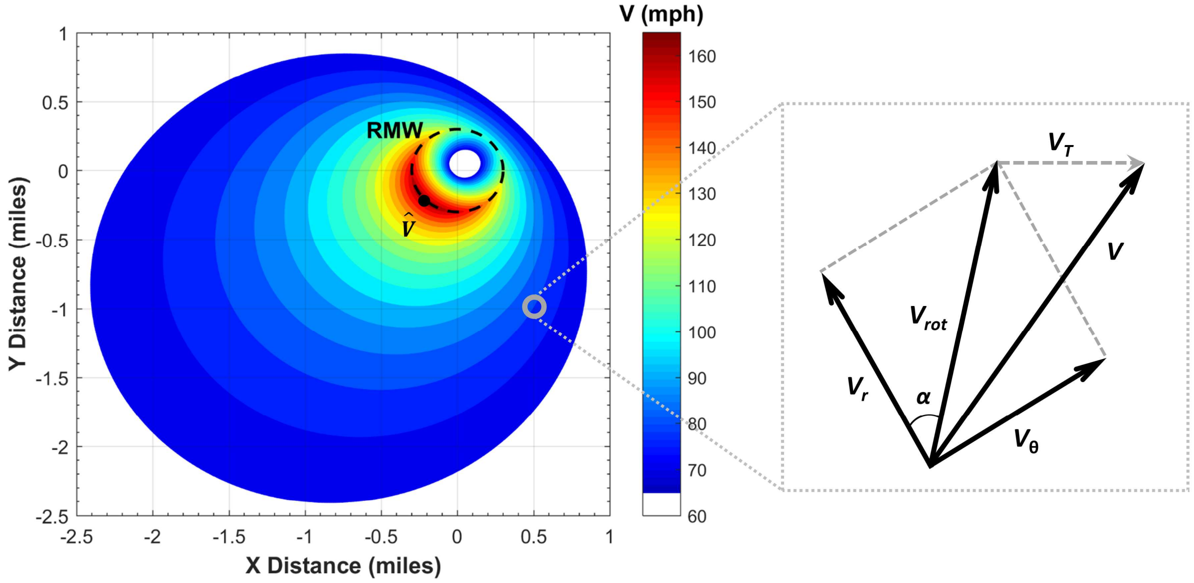

Figure 2. A translating tornado vortex on a grid (left); and wind components (V_r, V_θ, and V_T) and the resultant wind speed (V) (right) at a specific point. Note the translation direction of tornado is left to right. (V_t = 30 mph, G_{max} = 4.5, RMW = 0.3 miles, α = 45°, φ = 0.55). Wind speed below 65 mph (below EF-0) is not colored. The point of maximum overall wind speed ($\hat{V}$) is also shown.

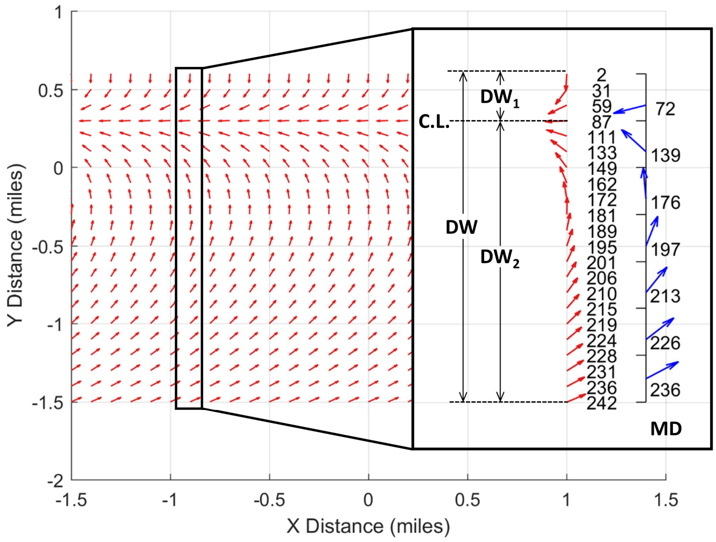

Figure 3. Tree-fall pattern produced by the translating tornado vortex in Fig.2 (left) with V_c = 85 mph; Illustration of *DW*, *DR*, and *MD* (right). DW_1 and DW_2 denotes the *DW* on the north and south side of the convergence line (C.L.), respectively. $DR = DW_2/DW_1$. Note that a grid spacing of 0.1 miles is used in the simulation and an average spacing of 0.3 miles is used for *MD*.

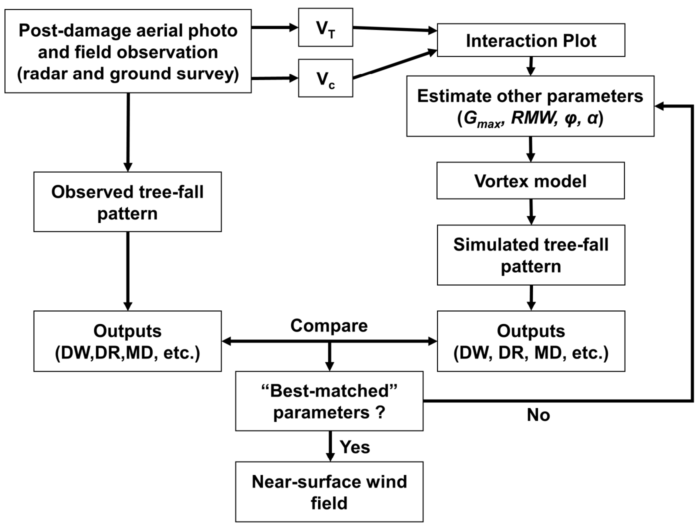

Figure 4. Generic tree-fall analysis process from aerial photo and observation to near-surface wind field estimation.

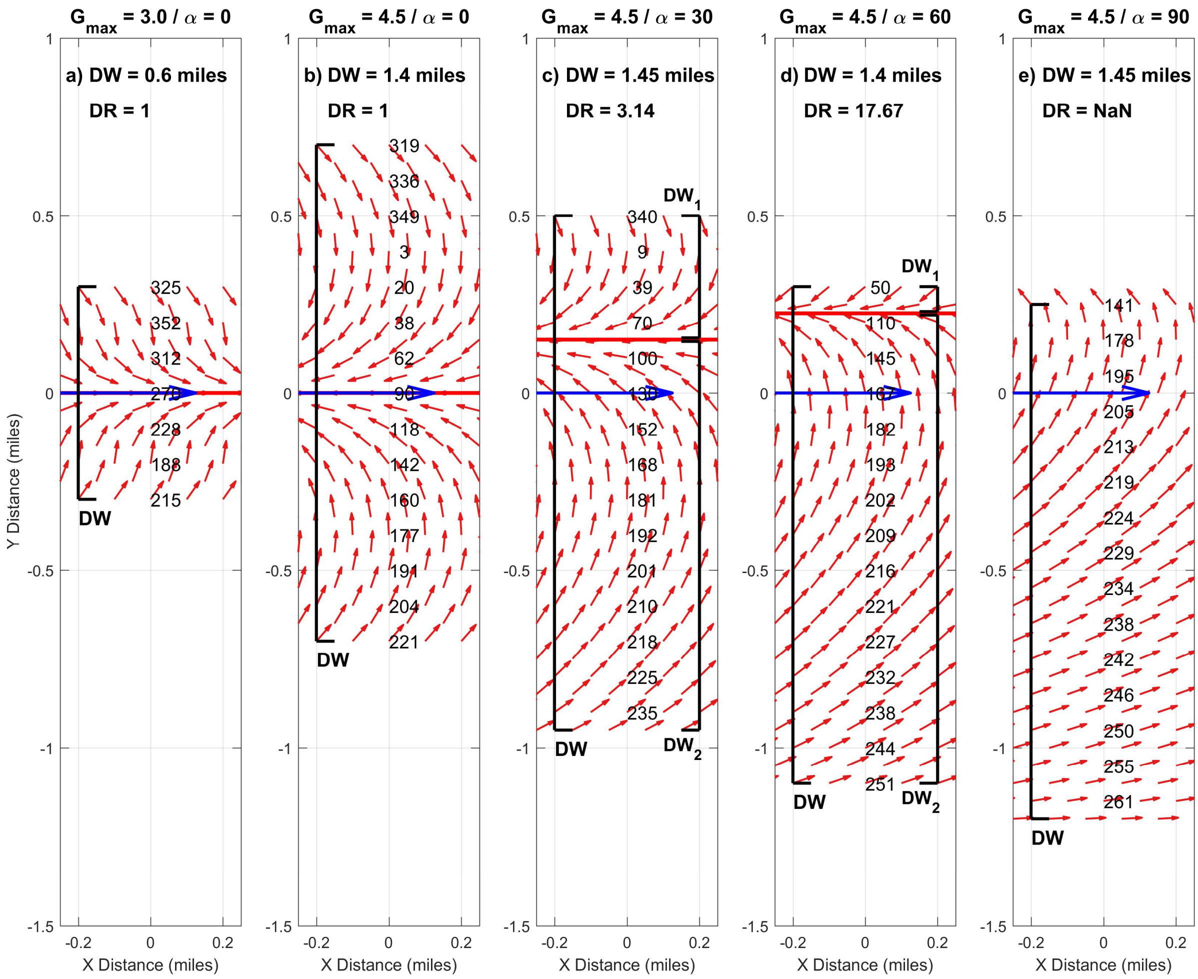

Figure 5. Examples of tree-fall pattern with different G_{max} (4a-4b) and α (4b-4e). Note that the tornado vortex is moving from left to right (blue arrow) and parameters not shown in the figure were kept constant (V_T = 30 mph, RMW = 0.2 miles, φ = 0.5, V_c = 85 mph). Convergence line is indicated in red line and the fall directions are labeled at x = 0 where 0 degree is due the true south and increases clockwise. A grid spacing of 0.1 miles is used for the simulation for illustration purposes.

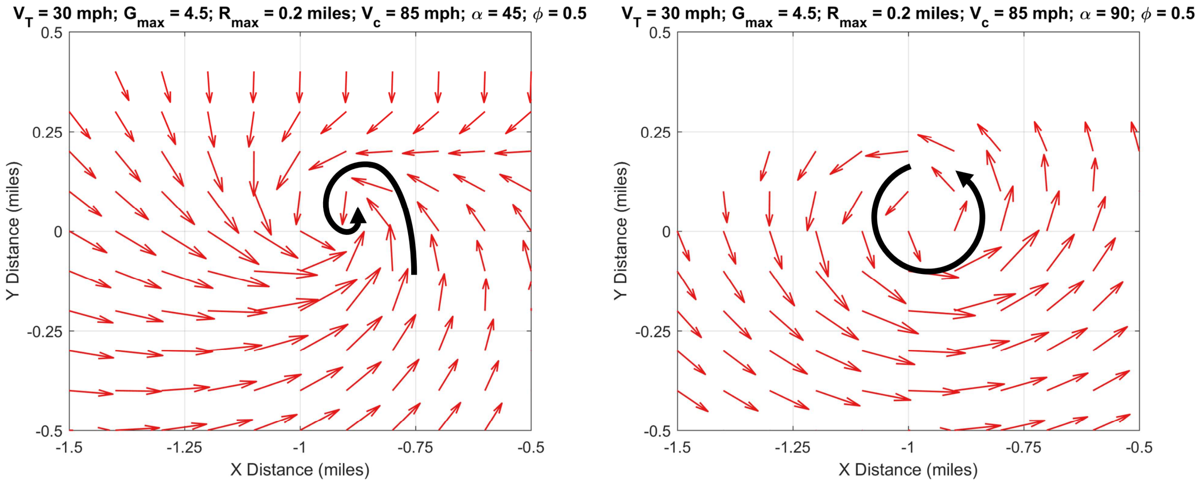

Figure 6. Examples of the simulated fall pattern in the beginning of the tornado that resembles "comma-shape" (left) and "swirling" (right) pattern. The parameters used for the simulation are written on top of each figure.

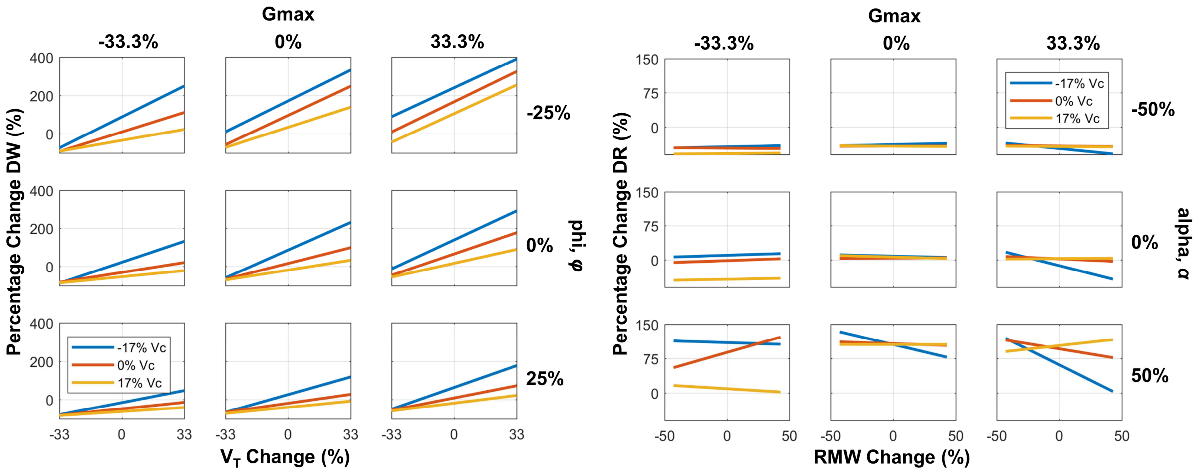

Figure 7. Example of interaction plot of *DW* (left) and *DR* (right). Note that the reference parameters to percentage change are: (1) $V_T = 30$ mph, $G_{max} = 4.5$, phi (φ) = 0.8, $V_c = 60$ mph (left); and (2) $G_{max} = 4.5$, $V_c = 60$ mph, alpha (α) = 30, $RMW = 0.35$ miles (right). The following parameters are fixed for each plot: (1) $\alpha = 15°$, $RMW = 0.3$ miles (left); and (2) $\varphi = 0.8$, $V_T = 30$ mph (right).

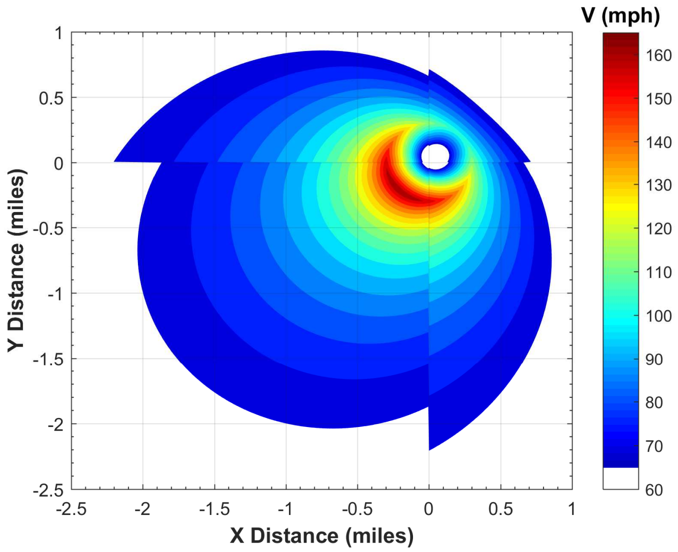

Figure 8. A translating tornado vortex (Fig .2) with different RV parameters used in each quadrant. $\varphi_1 = 0.5$, φ_2, $\varphi_4 = 0.55$, $\varphi_3 = 0.6$, where the subscript denotes the quadrant. Note that wind speed below 65 mph (below EF-0) is not colored.

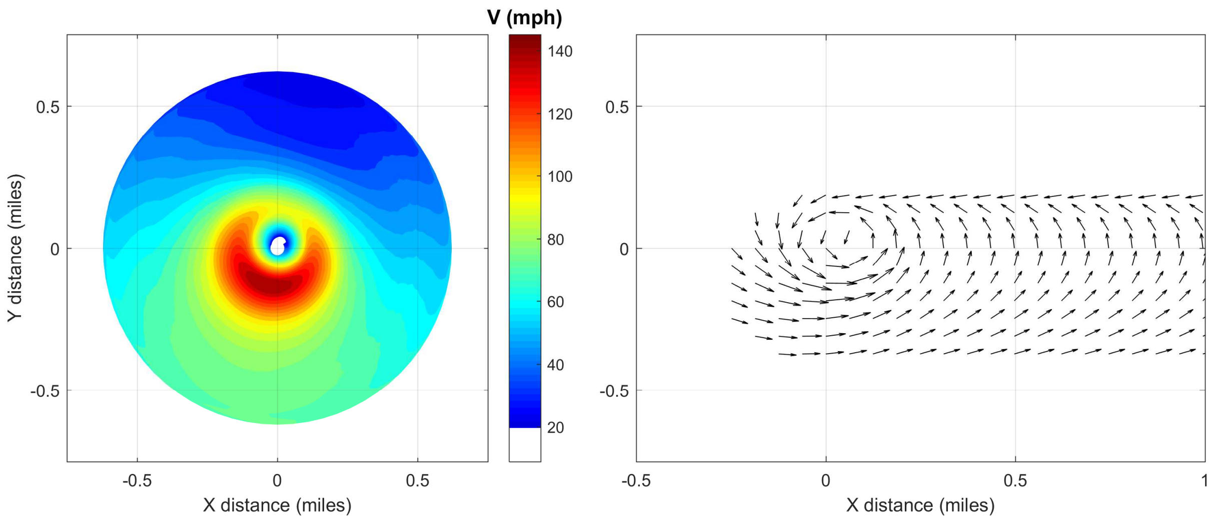

Figure 9. Radar velocity field (left) of the Stockton, KS tornado. Hypothetical tree-fall pattern (right) produced by translating the radar velocity field. Note that the vortex was dropped at (0,0) and translated from left to right and the critical wind speed of tree-fall (V_c) of 80 mph was used.

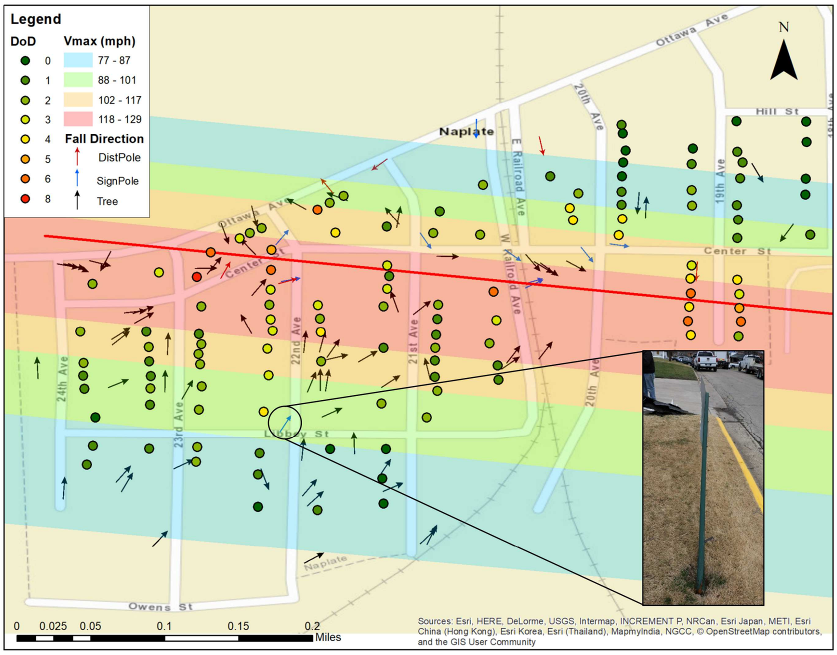

Figure 10. Damage survey map of Naplate, IL tornado over laid with the wind field (contour) produced from the tree-fall analysis. Residential houses (circles) are color coded according to its DOD rating. Tree-fall (black), distribution pole (red), and street-signs (blue) fall directions are shown in arrows. Note that the tornado is moving from left to right (red line indicates estimated tornado center). Example of street sign failure shown in bottom right.

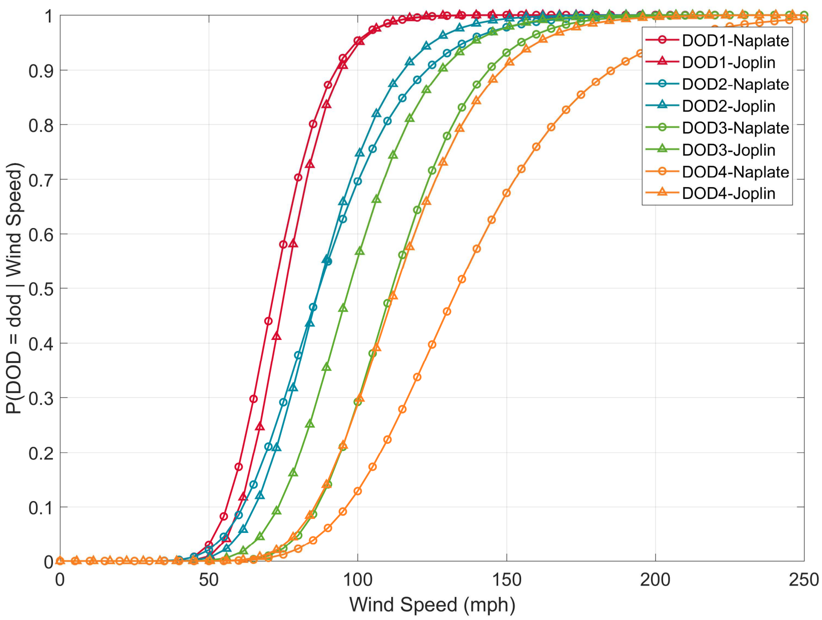

Figure 11. Empirical fragility curves of degrees of damage (DOD) for FR12 (one- and two-family residences) of Naplate, IL and Joplin, MO tornado.

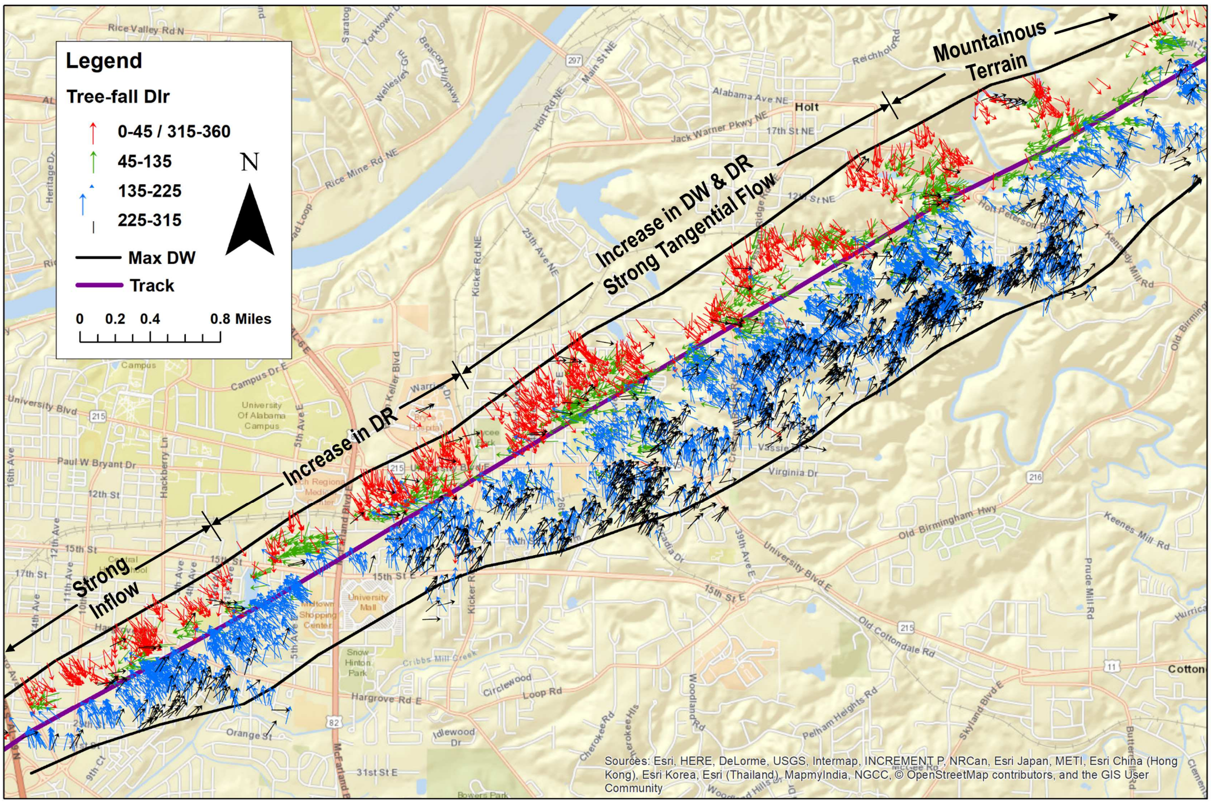

Figure 12. Direction of tree-fall from Tuscaloosa-Birmingham tornado. The arrows are color coded based on the tree-fall direction normalized by the direction of the tornado track. The tornado moved from southwest to northeast.

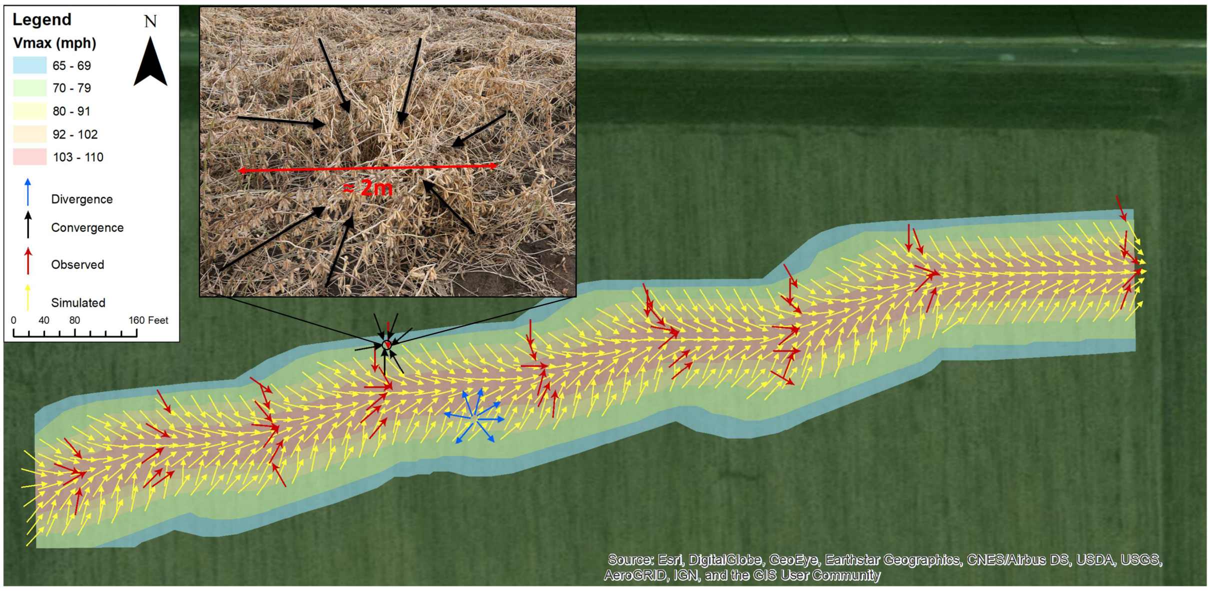

Figure 13. Crop-damage survey map of Sidney, IL tornado over laid with the wind field (contour) produced from the tree-fall analysis. Observed (red), including convergent (black) and divergent (blue), and the simulated (yellow) soybean-fall patterns are shown in arrows. Note that the tornado is moving from west to east and the convergent and divergent patterns are not drawn in scale.

TABLES

Table 1. “Best-matched” parameters for Naplate, IL tornado (left) and Sidney, IL tornado (right)

Naplate, IL Tornado		Sidney, IL Tornado	
Parameters	“Best-matched” value	Parameters	“Best-matched” value
G_{max}	1.5	G_{max}	2.2
Alpha (α)	27.5	Alpha (α)	5.0
RMW (m)	95	*RMW* (m)	12.5
Phi (φ)	0.75	Phi (φ)	0.65
V_c (m/s)	34	V_c (m/s)	36